One-Step Systemic Staging for Patients with Breast Cancer

20

Giuseppe Petralia and Anwar R. Padhani

20.1 Background

Despite advances in the treatment of primary breast cancer, metastatic spread of the disease remains a substantial clinical burden. Nearly 30% of breast cancer patients already have tumour spread to regional lymph nodes at diagnosis, and 5% will have metastases at presentation [1]. The prevalence of metastatic disease has increased along with the duration of survival, with some 20% of patients developing metastases during the course of the disease [2].

Breast cancer commonly metastasizes to the lymph nodes, bone, liver, lung and the central nervous system [3]. Of these, bone is the most frequent, being the first site of metastasis in more than 50% of the cases of relapsing disease [4], and present at the time of death in over 70% of those patients who die of breast cancer [5].

In order to effectively manage metastatic breast cancer patients, it is essential to have consistent, reproducible and validated methods for the detection of metastatic disease and for the evaluation of therapy response. These methods include clinical assessments, serum biomarkers and imaging techniques.

20.2 Clinical Assessments

Clinical assessments addressing pain, energy levels and mobility, often by means of questionnaire tools [6], are for the most part in the form of structured measures of quality of life. Although widely used in clinical trials, these questionnaires are not integrated into daily practice.

G. Petralia, M.D. (✉)
Divisions of Radiology, European Institute of Oncology, Milan, Italy
e-mail: giuseppe.petralia@ieo.it

A.R. Padhani, M.B.B.S., F.R.C.P., F.R.C.R.
Paul Strickland Scanner Centre, Mount Vernon Hospital, Northwood, Middlesex, UK

20.3 Serum Biomarkers

The serum biomarkers applied to the evaluation of metastatic breast cancer include CA 15.3, the oncofoetal protein carcinoembryonic antigen (CEA), the oncoprotein HER-2/neu and the cytokeratin tissue polypeptide-specific antigen (TPS) [7]. Although serum biomarkers are helpful in the detection of recurrent disease, they perform variably in the evaluation of treatment response [8] and are not useful for evaluating heterogeneous response across different metastatic sites.

Serum biomarkers of bone heath are complementary and seem to be particularly useful in patients who have bone disease that is difficult to assess by means of other methods [9]. Markers such as N-telopeptide of type I collagen (NTX) and bone-specific alkaline phosphatase (BAP) are related to osteoclastic/osteoblastic bone activity, respectively, and their elevation or reduction (in the case of NTX) has been related to increased or diminished risk of developing skeletal-related events, as well as being correlated to survival [10, 11].

Of increasing recent interest for assessing therapy response is the use of circulating tumour cells (CTCs) and circulating tumour cell-free DNA. It has been demonstrated that levels of CTCs at baseline and after chemotherapy are predictive of progression-free survival and overall survival in metastatic breast cancer [12, 13]. However, changing therapy on the basis of persistently elevated CTC levels despite treatment does not bring an increase in overall survival [14]. CTC evaluations have demonstrated an advantage over conventional radiological studies for predicting overall survival, but show low correlation with radiographic tumour load [13]. Circulating tumour cell-free DNA has shown early promise, and there is evidence of superiority to CTCs, in small studies of treatment response assessment in metastatic breast cancer [15]. Guidelines from the International Consensus Conference for Advanced Breast Cancer, therefore, state that changes in serum biomarkers alone should not be used alone to initiate changes in treatment [16].

U. Veronesi et al. (eds.), *Breast Cancer*, DOI 10.1007/978-3-319-48848-6_20

20.4 Imaging

20.4.1 Bone Scintigraphy (BS)

Planar bone scans with 99mTc-MDP (technetium-99m-methylene diphosphonate) are useful for the identification of metastatic bony disease as they have acceptable sensitivity [17]. Modern extensions to BS with SPECT or CT-SPECT improve bone scan performance [18, 19]. It is important to remember that 99mTc-MDP is bound to the bone as part of osteoblastic activity [20], and so BS does not necessarily reflect the full burden of disease within bone marrow space. In particular, pure lytic bone changes without an osteoblastic reaction may be missed (Fig. 20.1). In addition, it is impossible to assess patients with very advanced bone disease objectively because new disease cannot be confidently identified on the background of already elevated bone scan uptake (so-called superscans).

The utility of BS to positively identify response (as opposed to stable/progressive disease) is severely limited, because reductions of bone activity occur late in responding patients, which compromises the timeliness of bone scan readouts. Moreover, it is recognized that isotope BS can show transient increases in the size of detected lesions or new lesions in patients who are later shown to be responding to therapy (*flare reaction*) [21]. The biological explanation for the flare reaction is that successful treatment leads to osteoblast healing, which increases MDP uptake. The evaluation of response to therapy using BS is thus indirect (not reporting on tumour cell kill), and there is no evidence that bone scans may be used to assess positive therapy benefits [22].

20.4.2 Computed Tomography (CT)

Computed tomography (CT) is superior to bone scintigraphy for detecting bone disease [18]. CT scans allow measurement of the size of body metastases, extent of disease involvement and quantification of response to treatment, particularly of soft tissue disease. While CT measurements of soft tissue disease are incorporated into the RECIST [23], bone metastases are considered non-evaluable/measurable according to these criteria. Under RECIST, therefore, CT scans are used to assess response to treatment only for those bone metastases that have a measurable soft tissue component. The MD

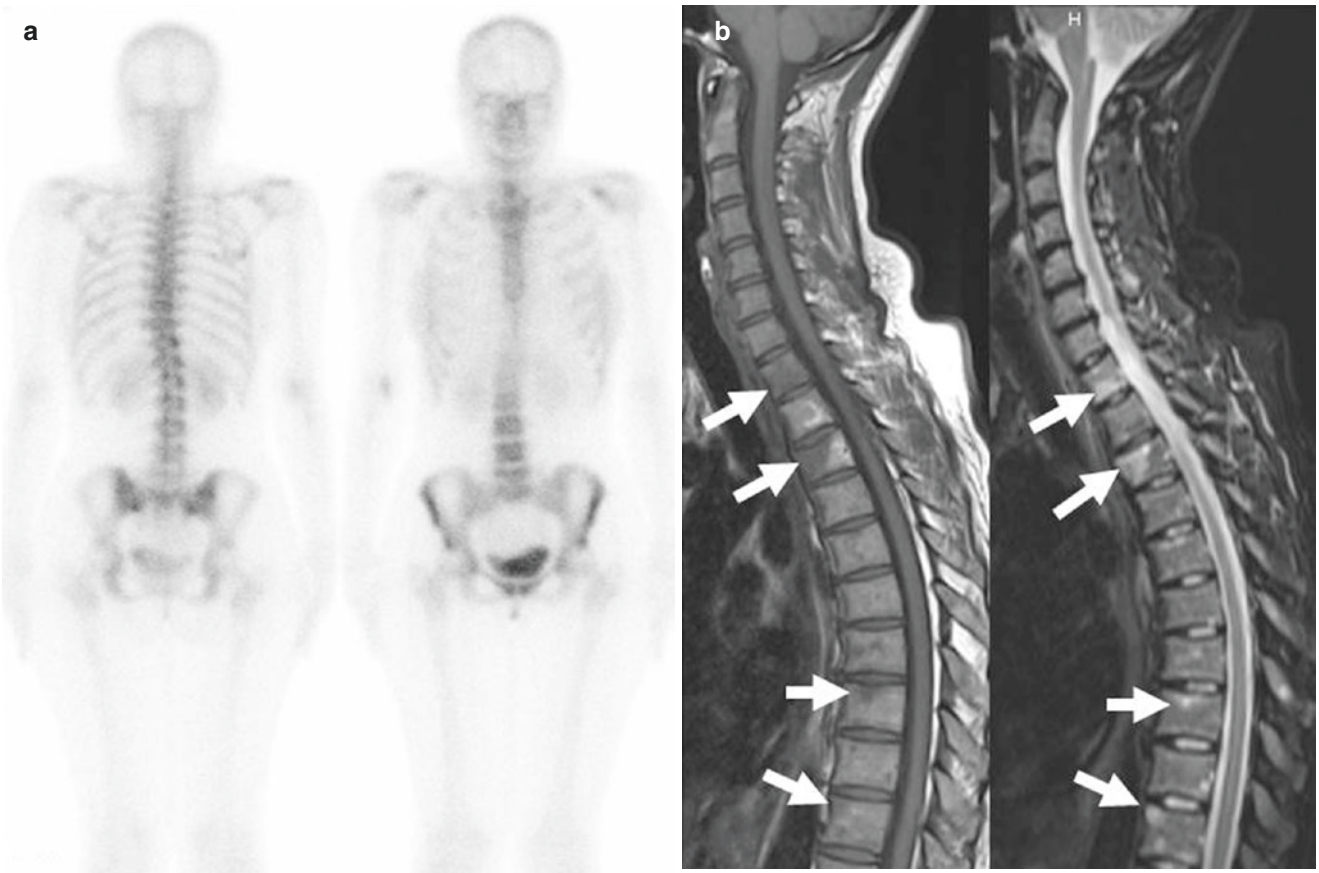

Fig. 20.1 Pure lytic bone metastases may not be apparent on bone scans. In this 43-year-old woman with nodal and liver metastases from breast cancer, 99mTc-MDP results were negative (**a**). In T1- and T2-weighted MRI of the spine performed 5 days later, multiple bone deposits can be seen (**b**—*arrows*). The large metastases in the thoracic spine show distinctive lytic features on MRI (*arrows*)

Anderson Cancer Centre criteria [24] have defined other CT features for defining response to treatment, which are based on the changes in bone structure and density within lesions. According to these criteria, an osteosclerotic reaction of a lytic/infiltrative lesion can be used as an indicator of response, as it can represent a healing process which again needs osteoblastic action (Fig. 20.2). Using the MDA criteria, the development of new osteosclerotic lesion(s) should not be classified as progression unless there is other evidence of disease progression. Unfortunately, these criteria have a significant limitation, as they are not applicable in breast cancer patients who receive anti-osteoclastic therapy (bisphosphonates), which are standard of care medicating in the metastatic setting.

20.4.3 Positron Emission Tomography (PET)

Positron emission tomography (PET) is an established technique for the diagnosis of distant metastases in breast cancer. It has potential advantages over anatomical imaging in that it demonstrates changes in metabolic activity that may occur prior to the changes in morphology depicted in CT. PET offers several different radiotracers for bone (^{18}F-NaF) and bone marrow imaging (^{18}F-FDG is the most commonly used marrow agent in breast cancer). ^{18}F-FDG PET has a strong role in evaluating metastatic disease that has accelerated glucose metabolism [25]. Unfortunately, in up to 42% of all oncological patients have FDG non-avid disease that is not appropriate for evaluation with ^{18}F-FDG PET [26]. In the setting of breast cancer, lobular cancer is oftentimes ^{18}F-FDG PET negative. ^{18}F-FDG PET data acquisition is usually coupled with CT for attenuation correction and anatomical correlation. The overall sensitivity and specificity for skeletal metastases detection of ^{18}F-FDG PET/CT are superior to those of CT and BS [27]. The role of PET/CT for monitoring bone response to therapy has been reported in a few, promising but small-scale studies [28]. Amongst the recognized limitations include the *flare* phenomenon; bone marrow "flare" reactions have been described for FDG PET/CT when bone marrow growth factors such as granulocyte colony-stimulating factor (G-CSF) are administered. In specific cases, the observation of a flare reaction could indicate therapy success, such as after the start of tamoxifen/fulvestrant therapy (usually after 7–10 days) in oestrogen receptor-positive breast cancers [29, 30].

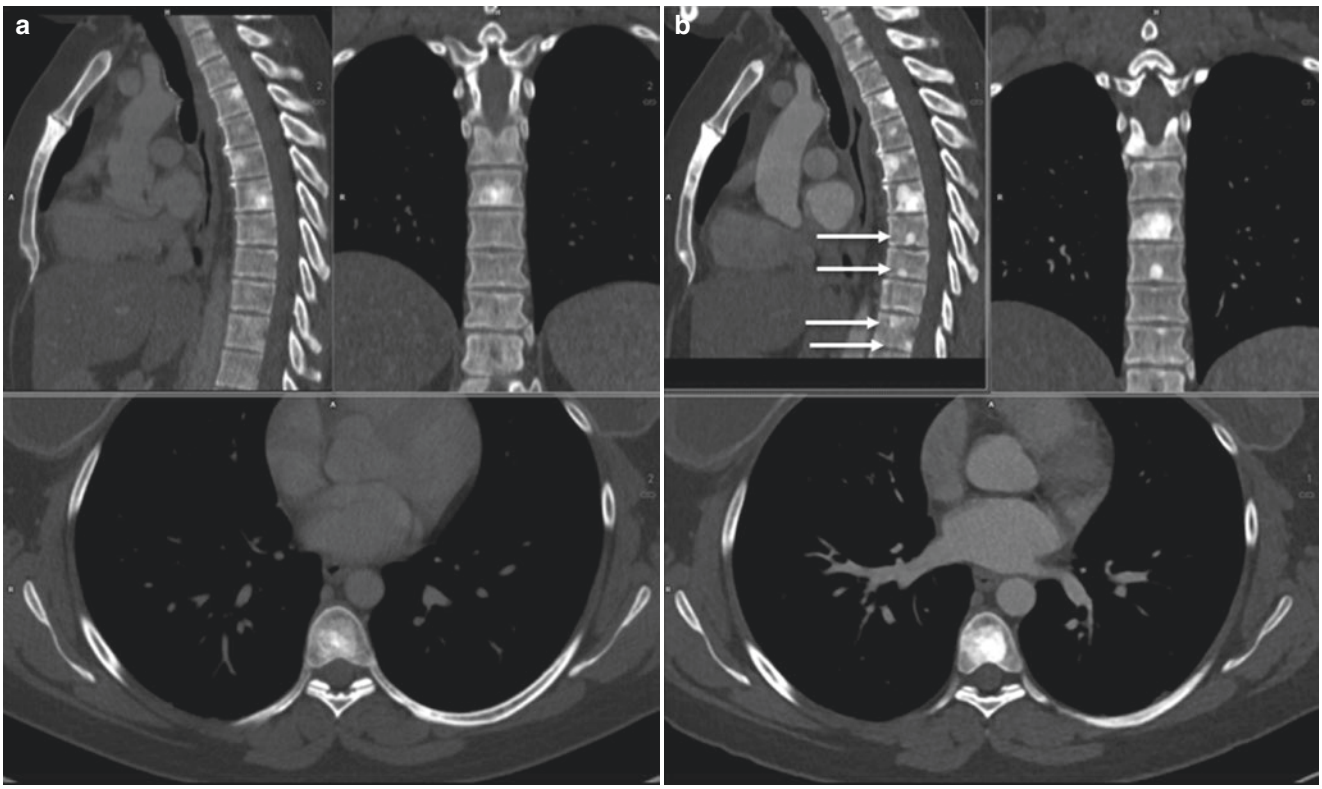

Fig. 20.2 Sclerotic response of bone metastases to therapy. A 35-year-old woman with BRCA-positive breast cancer and skeletal metastases has received prior, ineffective therapy with poly-ADP ribose polymerase (PARP) inhibitors. CT scans are acquired before and after new treatment with three cycles of carboplatin and bisphosphonates. Multiple metastases are visible in thoracic spine, some of them showing mixed sclerotic/lytic features (**a**). Dense sclerotic reaction can be seen in (**b**) in all lesions, likely indicating effective response to therapy. New, small sclerotic lesions have appeared in the second scan (*arrows*), suggesting response to therapy of smaller metastases that are not present/visible in (**a**)

20.4.4 Magnetic Resonance Imaging (MRI)

Magnetic resonance imaging (MRI) has a growing role in the diagnosis and assessment of response of metastatic disease and in particular bony disease. The key advantage of MRI is that the bone marrow can be directly evaluated using a variety of sequences each sensitive to different aspects of bone and bone marrow, such as the marrow cellular density (diffusion-weighted imaging (DWI) MRI), vascularity (dynamic contrast-enhanced (DCE) MRI) (diffusion-weighted imaging (DWI)), trabecular bone density (ultrashort echo time MRI and susceptibility-weighted MRI) and bone marrow fat:water ratio (Dixon MRI, MR spectroscopy). Another advantage of MRI is the ability to perform multiregion examinations including whole-body studies. Furthermore, techniques can be combined thus enabling morphologic and functional (sometimes quantitative) assessments of tumour response, which can be repeated as required, as there is no radiation exposure penalty. Advantages of MRI include the fact that no ionizing radiation is administered, no injection of isotopes is necessary and whole-body examinations are possible.

Several meta-analyses show that the performance of MRI is comparable to ^{18}F-FDG PET, both being significantly more accurate than bone scintigraphy and CT for detecting bone metastases in many types of cancers, on a per patient and per lesion basis [27, 31, 32]. MRI also performs well for monitoring therapy response of metastatic breast cancer patients using bone-specific response criteria [33]. Progression criteria include increase in number/size of focal/diffuse areas of metastatic infiltration within normal marrow, evolution of focal lesions to a diffuse neoplastic pattern and the appearance of or increases in soft tissue components associated with bone disease. The appearance of new fractures (needing radiotherapy/surgical interventions) should be considered as progression only if the bone marrow MRI signal intensity in the affected area is indicative of malignancy.

Amongst the findings considered indicative of bone lesion response are the emergence of intra-/peritumoural fat within/around lesions (*fat dot* and *fat halo* signs), decreases in contrast enhancement and the development of dense lesion sclerosis on T2-weighted fat-suppressed MR images.

There is however limited evidence for the use of morphologic MRI criteria for the assessment of bone response to treatment. Instead, a few small studies have identified problems with the use of morphologic descriptors of response, including arrested resolution of abnormalities despite effective therapy (presumed to be due to bone sclerosis, due to marrow fibrosis or due to necrosis). Other limitations of morphologic imaging include the problem of evaluating disease activity against an already scarred background and the so-called "T1W image pseudoprogression" phenomenon that occurs due to intense bone oedema secondary to massive cell death and inflammation, which can lead to darkening of the bone marrow on T1-weighted sequences, mimicking metastatic spread through the affected segments. Ollivier and colleagues have described these technical bone marrow changes in some detail [34], but the clinical data for the use of morphological MRI in the routine assessment of metastatic bony disease response are still lacking.

20.4.4.1 Diffusion Whole-Body (DWB) MRI

Diffusion whole-body (DWB) MRI is emerging as a promising bone marrow assessment tool for detection and therapy monitoring of bone metastases [35–37]. DWB MRI continues to make use of anatomic T1 and T2 sequences for morphologic evaluation, but combines them with diffusion-weighted sequences, for the functional representation of cellular density within tissues (Fig. 20.3). Diffusion-weighted imaging evaluates the microscopic motions of tissue water and allows the calculation of water diffusivity (apparent diffusion coefficient (ADC)) that reflects the degree of freedom of water movement. Water diffusivity is determined by architectural tissue properties such as cellular density, cellular arrangements, vascularity, size of the extracellular space, tissue viscosity and nuclear:cytoplasmic ratio. Increased tumour cell proliferation tends to increase cell density while decreasing the volume of the extracellular space, resulting in reductions of ADC values [38]. Importantly, due to technological advances, DWB MRI can be performed in clinically acceptable examination times (20–30 min depending on scanner capabilities); actual scan times are longer when combined with morphologic sequences (generally 40–50 min) [35–37].

20.4.4.2 Detection of Metastases

DWB MRI is attractive for metastatic lesion detection because diffusion-weighted imaging permits at a glance assessments of the entire body, immediately drawing attention to potential abnormal skeletal and body regions and thus helping to reduce image interpretation times of anatomic MRI [36]. On diffusion-weighted imaging, lytic/infiltrative skeletal metastases appear as focal or diffuse areas of high-signal intensity on high b-values (such as b900 s/mm^2, i.e. strongly weighted diffusion images) on a background of lower signal intensity of the normal bone marrow. It is important to emphasize that metastasis detection on diffusion-weighted images should not be done in isolation but rather has to be considered as a potent adjunct to the anatomical MRI assessments, the combination of which form a complete DWB MRI assessment [39]. This assertion has been highlighted in a recent meta-analysis demonstrating that DWI alone is a sensitive but rather unspecific tool for the detection of bone metastases [40]. Thus, the pooled sensitivity/specificity of DWI alone has been reported as 87.7% (95% confidence interval [CI]: 76.3–94.9%) and 86.1% (95% CI: 79.2–91.4%), compared to 90.9% (95% CI: 84.3–95.4%) and 96.1% (95% CI: 92.2–98.4%) for whole-body MRI without DWI [40].

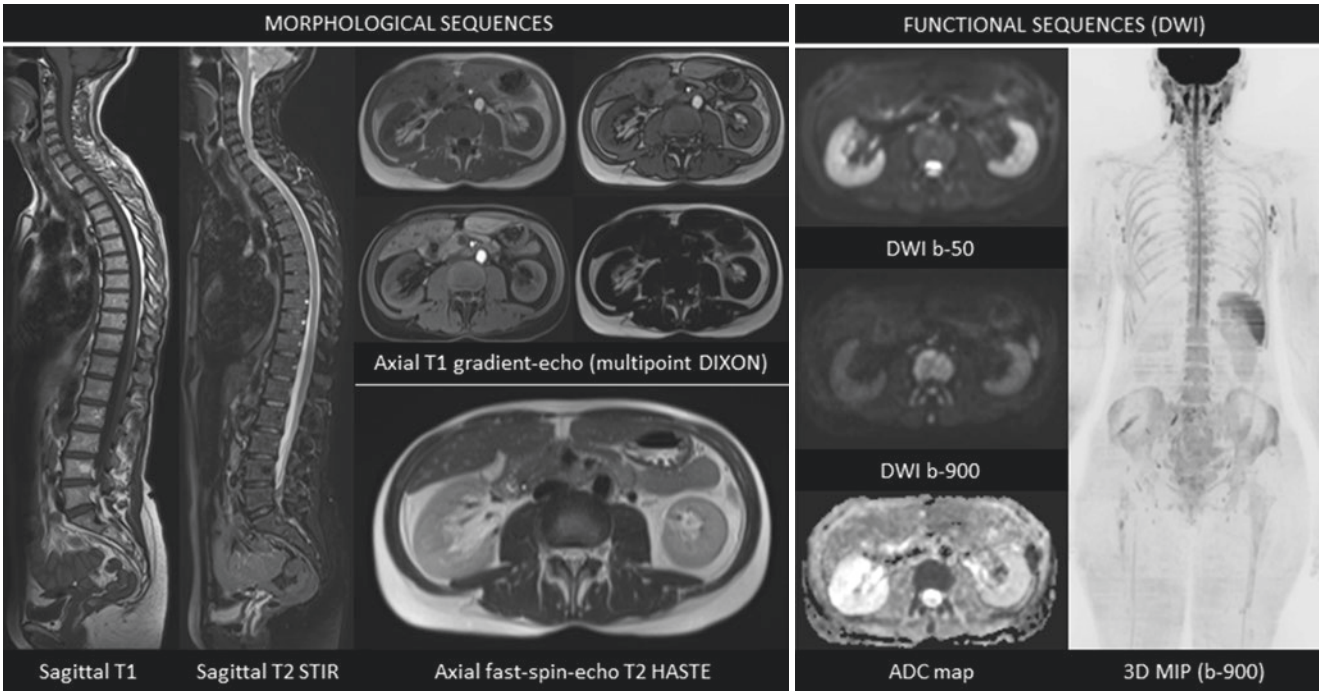

Fig. 20.3 Diffusion whole-body MRI consisting of sagittal T1-weighted and T2-weighted sequences on the whole spine, axial T1-weighted (multipoint DIXON), T2-weighted and diffusion-weighted images from head to mid-thigh, performed on a 1.5 T scanner (Magnetom Avanto, Siemens Healthcare Sector, Erlangen, Germany). Anatomy-specific phased-array surface coils are used for all body regions. The images are processed on a dedicated workstation (Leonardo, Siemens Healthcare Sector, Erlangen, Germany) to produce a unified axial series covering from head to mid-thigh and greyscale apparent diffusion coefficient (ADC) maps. Maximum intensity projections (MIPs) around the crania-caudal axis are generated from axial b900 s/mm^2 series and displayed in an inverted greyscale

Possible causes of increased skeletal signal intensity on high b-value images that lead to false-positive findings include bone marrow oedema caused by trauma [41], degenerative joint disease, bone infarction, infection and haemangiomas, isolated red bone marrow islands within yellow marrow and patchy bone marrow hyperplasia due to bone marrow growth factors. It should be noted, however, that a reader's experience, consideration of ADC values corresponding to hyperintensities on high b-value images and reference to the morphologic T1- and T2-weighted MR images can help reduce false-positive findings. Possible sources of false-negative findings include metastatic lesions in the anterior ribs and within the sternum that are sometimes relatively less conspicuous than lesions found in the spine and paraspinal regions; at these sites, respiratory motion contributes to signal losses on high b-value images. Other causes of false-negative results in bone marrow tumour detection include low levels of tumour infiltration (myeloma or densely sclerotic metastases), location of metastases in the skull vault and skull base (due to the adjacent high signal intensity of the brain) and the development of metastases within hypercellular bone marrow. As a general rule, lytic bony metastases are better seen than pure sclerotic metastases because of the lower water and cellular content of sclerotic and treated lesions [42, 43].

A recent review showed that DWB MRI has overall equal performance to FDG-PET for detecting primary tumours and soft tissue metastases [44]. In addition, it has been established that the diagnostic performance of DWI in combination with conventional non-contrast T1- and T2-weighted imaging in detecting liver metastases (the second most common site of metastases) is high, comparable with contrast-enhanced MRI [45]. DWI has also shown good performance for lymph node assessment, as well as for detecting peritoneal/GI involvement, which are other common sites of metastases for breast cancer patients [46]. Thus, DWB MRI is indicated in all breast cancer patients, who need accurate staging of the entire body, including those at high risk of metastases at presentation (inoperable locally advanced breast cancer (T3/T4) patients and those with inflammatory cancer) or with early locoregional relapse. Another emerging application is the use of DWB MRI in pregnant women with breast cancer [47]. Due to their lowered immunity, diagnosis of advanced stage disease is 2.5 times more likely in these patients than in the general population [48], demanding for an accurate bone and liver staging. It is obvious that the absence of contrast agent and radiation exposure makes a DWB MRI the technique of choice in such patients. Finally, DWB MRI is increasingly used in breast cancer women below 35 years of age, to replace bone scan and abdominal-

pelvic CT scan, to avoid radiation exposure. It is well known that the estimated lifetime attributable risk of death from cancer dramatically increases in patients undergoing CT examinations prior to 35 years of age [49]. DWB MRI is often used when equivocal findings are observed with other techniques where non-FDG avid metastases may be present. Moreover, the other most common sites of metastases (after bone) in lobular breast cancer patients are GI organs, peritoneum and pleura; these sites that are difficult to evaluate with PET/CT, CT or ultrasound. Due to the high tissue contrast between hyper-cellular metastases and the suppressed background tissue, DWB MRI may facilitate detection of metastases in these sites (Fig. 20.4).

20.4.4.3 Monitoring Therapy Response

In the context of therapy monitoring, the attractions of DWB MRI are largely those mentioned above in regard to the absence of radiation and contrast agent with the added consideration that in the course of serial imaging, multiple episodes of radiation exposure are avoided. The absence of contrast agent administration in the majority of applications makes DWB MRI extremely useful in patients with impaired renal function, as well as helping to prevent gadolinium accumulation in the brain [50].

Therapy assessments with DWB MRI are largely made by observing changes in the volume and symmetry of signal-intensity abnormalities on high b-value images, together with changes in ADC values. Nonetheless, correlating the diffusion-weighted imaging findings with morphological appearances on conventional MR images (T1W, fat-saturated T2W/STIR and Dixon) remains important. The lower spatial resolution of diffusion-weighted images is not a real issue in daily practice, as accurate measurements of soft tissue lesions can be easily performed in corresponding axial T1- and T2-weighted images using RECIST or WHO criteria [23, 24]. Although monitoring of bone and soft tissue metas-

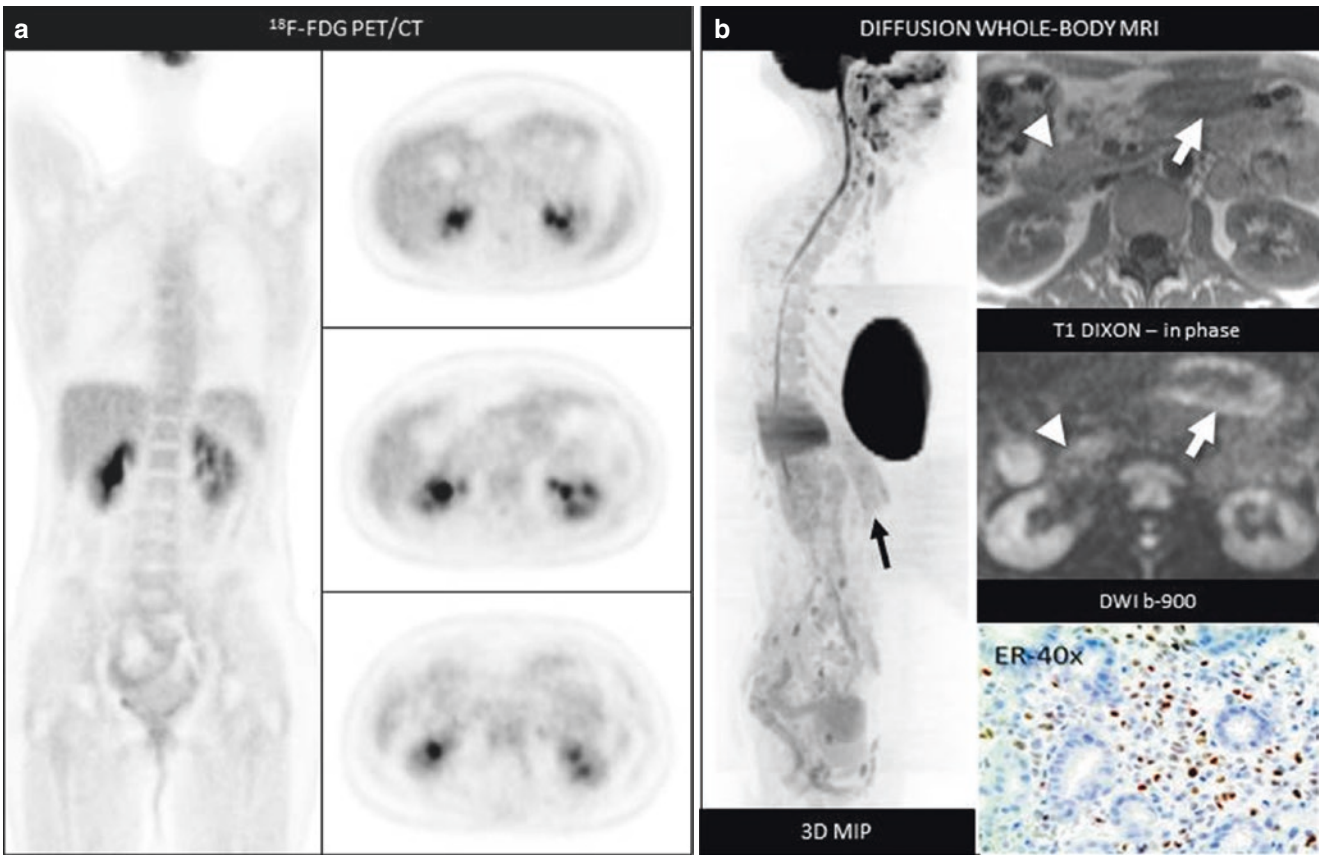

Fig. 20.4 Low sensitivity of 18F-FDG PET/CT for metastases from lobular breast cancer. A 44-year-old woman with operated lobular breast cancer is re-staged with 18F-FDG PET/CT due to suspicion of recurrence after progressive rise in CA 15.3. The FDG/PET examination was negative. After further rises in tumour markers, a second PET/CT (**a**) is performed 8 months later, confirming the absence of detectable disease. DWB MRI is performed at the same time point (**b**), with findings suspicious for the presence of abdominal metastases. Suspicious solid tissue on the right anterior renal fascia is visible both on the anatomical and diffusion-weighted sequences (*arrowheads*). In addition to this, in the DWI sequences abnormally high signal can be seen in the gastric walls (*arrows*): an anatomical site where signal is usually suppressed in b900 images. A second DWB MRI performed two months later confirms these findings. The patient undergoes gastroscopy and multiple punch biopsies of the gastric wall are taken, with positive results for the presence of infiltrating breast cancer (Image of the gastric infiltration for courtesy of Dr. G. Renne, IEO, Milan)

tases is generally based upon similar principles, the evaluation of changes in the bone is unique to DWB MRI, which involves a more detailed and specific process of image interpretation and analysis.

For the monitoring of bone metastases, the lesion-by-lesion signal intensity and ADC value changes can be interpreted using the guidance in Fig. 20.5 with several distinct patterns being recognized in the therapy assessment setting [51].

When bone metastases are treated successfully, the death of tumour cells results in cellular membrane destruction and liberation of intracellular water, which results in increases in water diffusivity, manifested as higher ADC values [52, 53] (generally above the threshold of 1400–1500 μm²/s). ADC increases may be greater for therapies that result in tumour cell death via necrosis rather than via apoptosis because of the associated inflammatory response [54], but this has not been definitively shown. As we have already noted, a prominent response mechanism is the development of dense osteoblastic lesions (osteoblastic scar), the sclerotic response category in Fig. 20.2. Regardless of the mechanism of tumour cell death, in the majority of lesions responding to therapy, high b-value images tend to show signal decreases (Fig. 20.6). Occasionally, however, a successful response to therapy with marked rise in ADC values may yield little change in high b-value signal intensity changes due to T2 shine-through (Fig. 20.7).

When bone metastases are not treated successfully, an increase in the volume of previously documented abnormal signal intensity on high b-value images is observed with new areas of abnormal signal intensity. Increases in the intensity of abnormalities on high b-value diffusion-weighted images can also indicate disease progression (Fig. 20.8).

Importantly, bony metastases that progress can have variable changes in ADC values, with modest increases, unchanged or slight decreases in ADC values compared to pre-therapy values that can occur [52, 55]. Reductions in

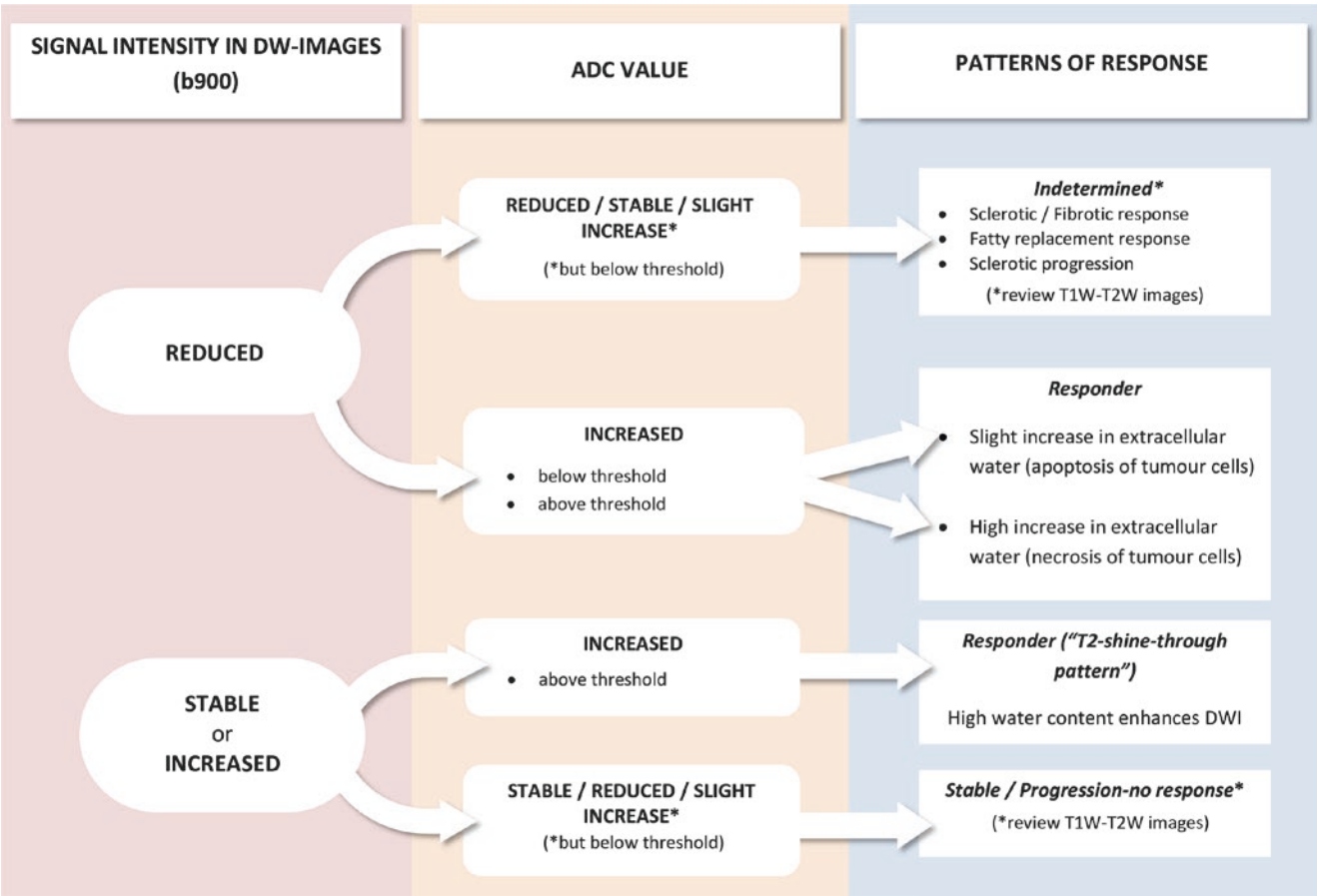

Fig. 20.5 Proposed scheme for assessing therapy response of bone metastases using diffusion-weighted MRI scans, ADC measurements and morphologic images [adapted from *Therapy Monitoring of Skeletal Metastases with Whole-Body Diffusion MRI*; Padhani AR et al. J Magn Reson Imaging 2014]

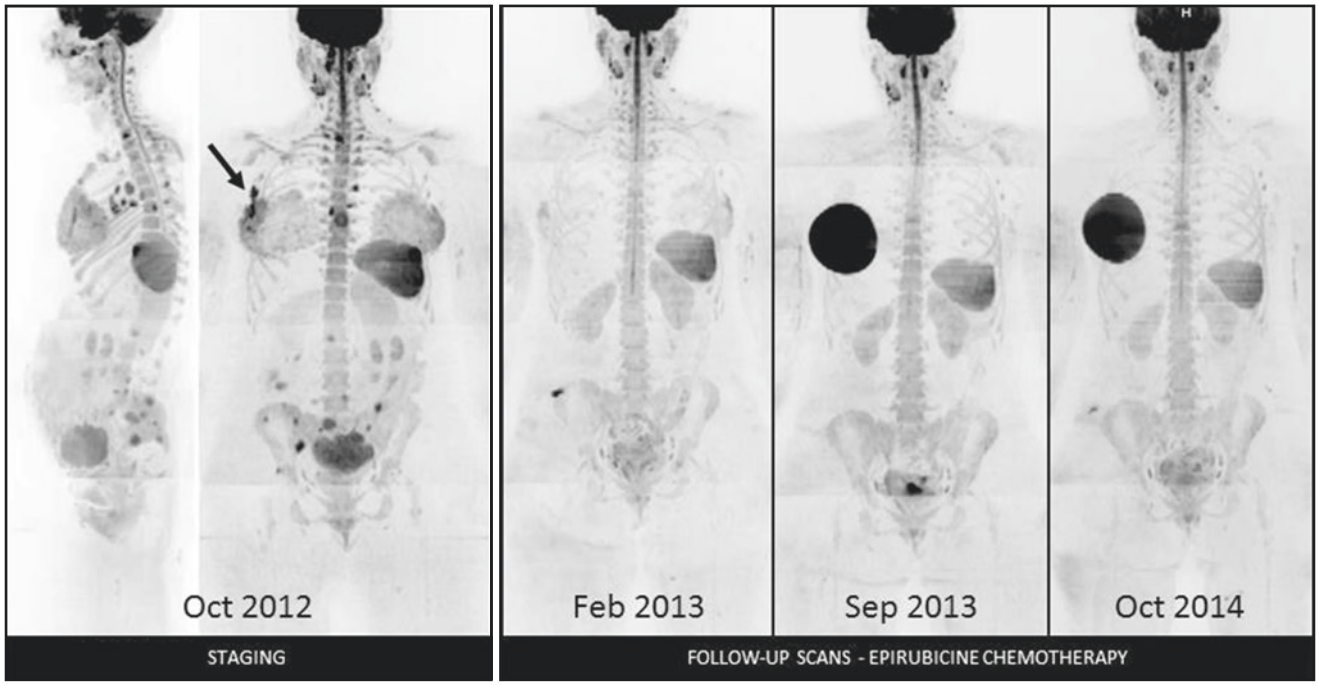

Fig. 20.6 Disease staging and follow-up in a 31-week-pregnant woman with newly diagnosed breast cancer. A pregnant 37-year-old woman is diagnosed with infiltrating breast cancer after fine-needle biopsy of a right breast solid lesion. DWB MRI at staging purpose (October 2012) revealed bone metastases in the dorsal and lumbar spine, in the pelvis and in the sternum. All of the lesions are visible in the rotational b900 MIP reconstruction. The brain, spinal cord and the kidneys of the foetus and mother are well visualized. The right primary tumour and right axillary lymph node enlargement can be seen (*arrow*). Chemotherapy was started after caesarean section. Follow-up scan on February 2013 after three cycles of chemotherapy shows complete response of the bone lesions, with loss of signal on b900 DWI images. All following DWB MRI follow-up scans confirmed a sustained, complete response to chemotherapy

ADC values are probably related to increasing cellularity within a fixed bone marrow space or due to bone sclerosis. Stable ADC values could occur with unchanged tumour cellularity accompanying increases in the geographic extent of disease. The causes for modest increases in ADC values with disease progression are related to increasing tumour infiltration, which displaces fat cells, increases bone marrow water (including water in the extracellular space) and increases tissue perfusion, thus returning higher ADC values compared to yellow or mixed bone marrow [42, 56–60]. ADC values in excess of 1400–1500 $\mu m^2/s$ are rarely seen with disease progression unless there is de novo tumour necrosis.

Further developments of DWB MRI include the quantitative tumour volume assessments that can be undertaken by segmenting high signal intensity regions on high b-value images. Corresponding whole-body ADC histograms can also be generated. Improved precision of response assessment can be undertaken by deriving "viable tumour volume" using threshold ADC cut-off values to exclude normal bone marrow (<600–650 $\mu m^2/s$) and non-viable necrotic tumour with ADC >1400–1500 $\mu m^2/s$ [42, 58]. The proportion of viable tumour can then be calculated and followed over time in the subsequent DWB MRI examinations.

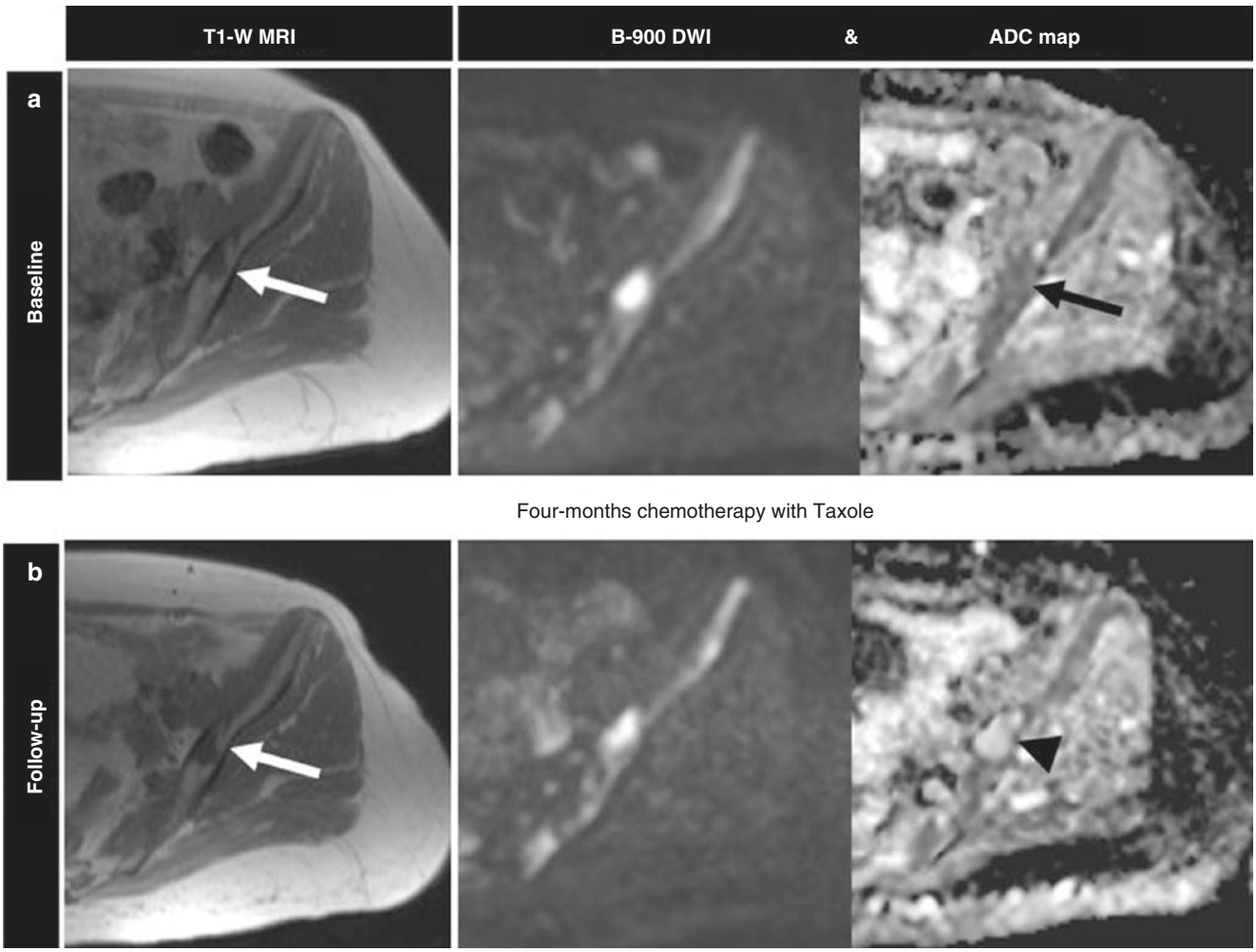

Fig. 20.7 T2 shine-through pattern indicating successful response to chemotherapy. A 51-year-old woman with bone-metastatic breast cancer undergoes DWB at baseline and after treatment with Taxol. (**a**) a metastatic lesion in the left iliac bone is shown as acquired in the baseline evaluation, on T1-weighted and b900 DWI images, as well as on the related ADC map. The lesion has a hypo-intense appearance on T1-weighted images (*white arrow* in **a**) and has a high signal on b900 images with corresponding low ADC values (*black arrow*), suggesting the presence of active disease. (**b**) A second evaluation with DWB after chemotherapy shows unchanged features of the metastasis in the T1-weighted images (*white arrow* in **b**). The lesion maintains high signal in b900 images. The ADC map of the lesion reveals a significant elevation in the mean ADC values (above 1500 $\mu m^2/s$, *black arrowhead*) indicating complete response to chemotherapy. The high signal in b900 images with accompanying high ADC values is termed "T2 shine-through"; the latter is strongly associated with cell necrosis and tumour response

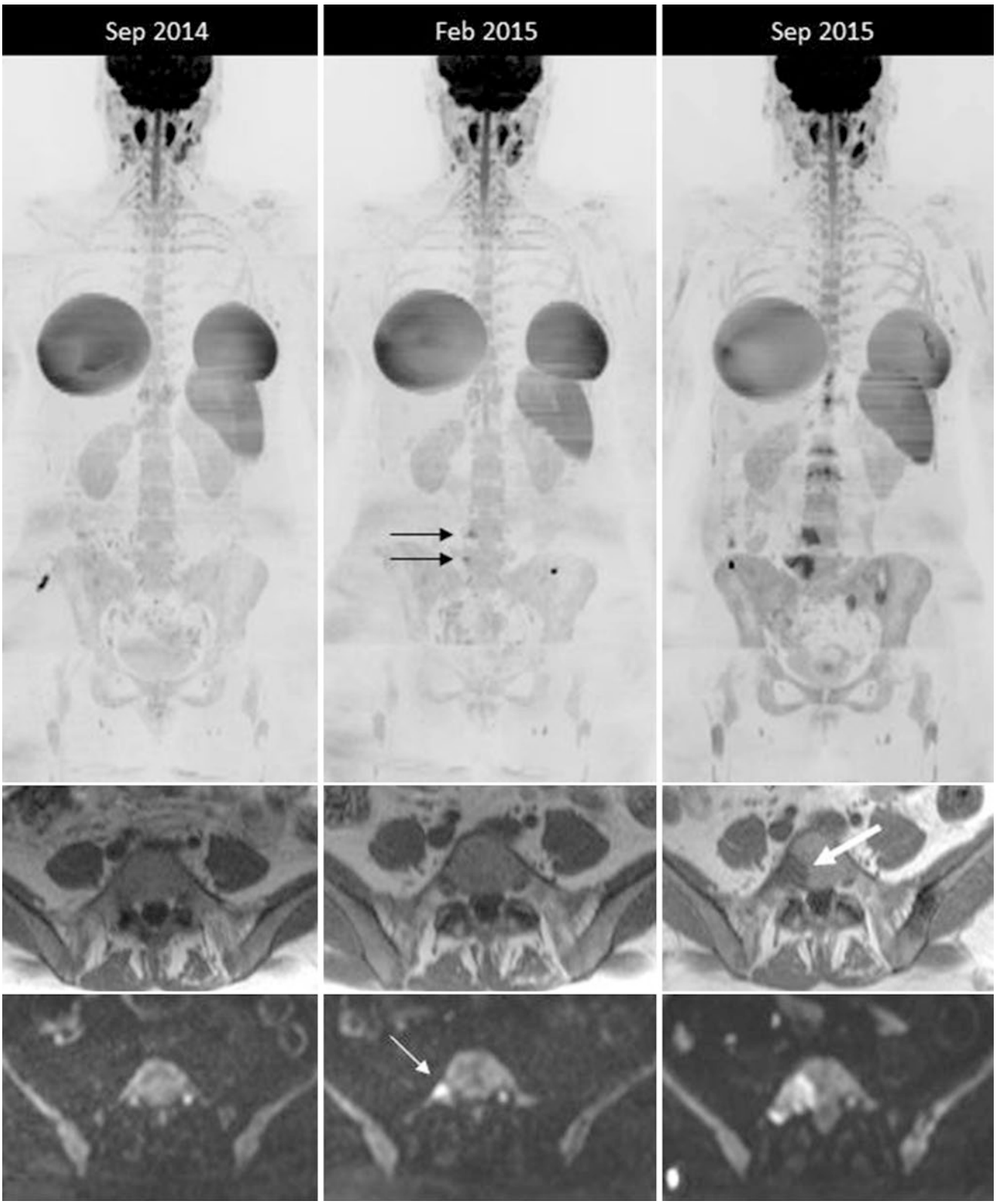

Fig. 20.8 Bone disease progression in anatomical and diffusion-weighted images. Serial changes in a 39-year-old woman with progressive metastatic breast cancer being treated with hormonal therapy and bisphosphonates. Axial anatomical (T1W) and DWI images (b900) and inverted coronal MIP images allow bone metastases to be evaluated over time. The second scan shows bone disease progression with re-activation of lesions not visible in examination 1 (*black arrows*). Increases in the number of lesions in the lumbosacral spine and pelvis are seen on examination 3. Axial images show re-activation and then growth of a bone metastasis located adjacent to the right sacroiliac joint despite therapy change in February 2015. Note the presence of a new lesion posteriorly in the left iliac bone adjacent to the left SI joint whose signal on high *b*-value images is being moderated by osteosclerosis

Conclusions

Whole-body MRI has the potential address the unmet clinical need for an accurate method to detect and monitoring response of all manifestations of metastatic breast cancer. There is a need to develop common measurements and analysis methods and to establish uniform data displays, to expand the use of quantitative analyses of DWB MRI in clinical practice. The technology is now mature enough to incorporate into clinical studies that define appropriate use of this technology.

Acknowledgements We would like to acknowledge the valuable contribution of Fabio Zugni (MD) in writing, literature search and figures editing.

References

1. National Cancer Institute. SEER fact sheet for breast cancer
2. American Cancer Society (2013) Breast cancer facts and figures. Internet
3. Kennecke H, Yerushalmi R, Woods R, Cheang MC, Voduc D, Speers CH, Nielsen TO, Gelmon K (2010) Metastatic behavior of breast cancer subtypes. J Clin Oncol 28(20):3271–3277
4. Ibrahim T (2013) A new emergency in oncology: bone metastases in breast cancer patients (Review). Oncol Lett 6(2):306–310. doi:10.3892/ol.2013.1372
5. Coleman RE (2006) Clinical features of metastatic bone disease and risk of skeletal morbidity. Clin Cancer Res 12(20):6243s–6249s
6. Cella DF, Tulsky DS, Gray G et al (1993) The functional assessment of cancer therapy scale: development and validation of the general measure. J Clin Oncol 11(3):570–579
7. Chuthapisith S, Eremin JM, Eremin O (2008) Predicting response to neoadjuvant chemotherapy in breast cancer: molecular imaging, systemic biomarkers and the cancer metabolome (Review). Oncol Rep 20(4):699–703
8. Tampellini M, Berruti A, Bitossi R et al (2006) Prognostic significance of changes in CA 15-3 serum levels during chemotherapy in metastatic breast cancer patients. Breast Cancer Res Treat 98(3):241–248
9. Duffy MJ, Evoy D, McDermott EW (2010) CA 15-3: uses and limitation as a biomarker for breast cancer. Clin Chim Acta 411(23–24):1869–1874
10. Brown JE, Cook RJ, Lipton A et al (2010) Prognostic factors for skeletal complications from metastatic bone disease in breast cancer. Breast Cancer Res Treat 123(3):767–779
11. Lipton A, Cook R, Saad F et al (2008) Normalization of bone markers is associated with improved survival in patients with bone metastases from solid tumors and elevated bone resorption receiving zoledronic acid. Cancer 113(1):193–201
12. Cristofanilli M, Budd GT, Ellis MJ et al (2004) Circulating tumor cells, disease progression, and survival in metastatic breast cancer. N Engl J Med 351(8):781–791
13. Budd GT, Cristofanilli M, Ellis MJ et al (2006) Circulating tumor cells versus imaging—predicting overall survival in metastatic breast cancer. Clin Cancer Res 12(21):6403–6409
14. Smerage JB, Barlow WE, Hortobagyi GN et al (2014) Circulating tumor cells and response to chemotherapy in metastatic breast cancer: SWOG S0500. J Clin Oncol 32(31):3483–3489. doi:10.1200/JCO.2014.56.2561
15. Dawson S-J, Tsui DWY, Murtaza M et al (2013) Analysis of circulating tumor DNA to monitor metastatic breast cancer. N Engl J Med 368(13):1199–1209
16. Cardoso F, Costa A, Norton L et al (2012) 1st International consensus guidelines for advanced breast cancer (ABC 1). Breast 21(3):242–252
17. Buscombe JR, Holloway B, Roche N, Bombardieri E (2004) Position of nuclear medicine modalities in the diagnostic work-up of breast cancer. Q J Nucl Med Mol Imaging 48(2):109–118
18. Even-Sapir E (2005) Imaging of malignant bone involvement by morphologic, scintigraphic, and hybrid modalities. J Nucl Med 46(8):1356–1367
19. Ben-Haim S, Israel O (2009) Breast cancer: role of SPECT and PET in imaging bone metastases. Semin Nucl Med 39(6):408–415
20. Brenner AI, Koshy J, Morey J et al (2012) The bone scan. Semin Nucl Med 42(1):11–26
21. Vogel CL, Schoenfelder J, Shemano I et al (1995) Worsening bone scan in the evaluation of antitumor response during hormonal therapy of breast cancer. J Clin Oncol 13(5):1123–1128
22. National Institute for Health and Clinical Excellence (NICE) (2009) Advanced breast cancer
23. Eisenhauer EA, Therasse P, Bogaerts J et al (2009) New response evaluation criteria in solid tumours: revised RECIST guideline (version 1.1). Eur J Cancer 45(2):228–247
24. Hamaoka T, Costelloe CM, Madewell JE et al (2010) Tumour response interpretation with new tumour response criteria vs the World Health Organisation criteria in patients with bone-only metastatic breast cancer. Br J Cancer 102(4):651–657
25. Torigian DA, Huang SS, Houseni M, Alavi A (2007) Functional imaging of cancer with emphasis on molecular techniques. CA Cancer J Clin 57(4):206–224
26. Iagaru A, Mittra E, Mosci C et al (2013) Combined 18F-Fluoride and 18F-FDG PET/CT scanning for evaluation of malignancy: results of an international multicenter trial. J Nucl Med 54(2):176–183
27. Yang H-L, Liu T, Wang X-M et al (2011) Diagnosis of bone metastases: a metaanalysis comparing ^{18}FDG PET, CT, MRI and bone scintigraphy. Eur Radiol 21(12):2604–2617
28. Lin NU, Thomssen C, Cardoso F et al (2013) International guidelines for management of metastatic breast cancer (MBC) from the European School of Oncology (ESO)-MBC Task Force: surveillance, staging, and evaluation of patients with early-stage and metastatic breast cancer. Breast 22(3):203–210
29. Dehdashti F, Flanagan FL, Mortimer JE et al (1999) Positron emission tomographic assessment of "metabolic flare" to predict response of metastatic breast cancer to antiestrogen therapy. Eur J Nucl Med 26(1):51–56
30. Mortimer JE, Dehdashti F, Siegel BA et al (2001) Metabolic flare: indicator of hormone responsiveness in advanced breast cancer. J Clin Oncol 19(11):2797–2803
31. Xu GZ, Li CY, Zhao L, He ZY (2012) Comparison of FDG whole-body PET/CT and gadolinium-enhanced whole-body MRI for distant malignancies in patients with malignant tumors: a meta-analysis. Ann Oncol 24(1):96–101
32. Li B, Li Q, Nie W, Liu S (2014) Diagnostic value of whole-body diffusion-weighted magnetic resonance imaging for detection of primary and metastatic malignancies: a meta-analysis. Eur J Radiol 83(2):338–344
33. Lecouvet FE, Larbi A, Pasoglou V et al (2013) MRI for response assessment in metastatic bone disease. Eur Radiol 23(7):1986–1997
34. Ollivier L (2006) Improving the interpretation of bone marrow imaging in cancer patients. Cancer Imaging 6(1):194–198
35. Takahara T, Imai Y, Yamashita T et al (2004) Diffusion weighted whole body imaging with background body signal suppression (DWIBS): technical improvement using free breathing, STIR and high resolution 3D display. Radiat Med 22(4):275–282
36. Kwee TC, Takahara T, Ochiai R et al (2009) Whole-body diffusion-weighted magnetic resonance imaging. Eur J Radiol 70(3):409–417

37. Padhani AR, Gogbashian A (2011) Bony metastases: assessing response to therapy with whole-body diffusion MRI. Cancer Imaging 11(1A):S129–S154
38. Yankeelov TE, Arlinghaus LR, Li X, Gore JC (2011) The role of magnetic resonance imaging biomarkers in clinical trials of treatment response in cancer. Semin Oncol 38(1):16–25
39. Koh DM, Blackledge M, Padhani AR et al (2012) Whole-body diffusion-weighted MRI: tips, tricks, and pitfalls. Am J Roentgenol 199(2):252–262
40. Wu L-M, Gu H-Y, Zheng J et al (2011) Diagnostic value of whole-body magnetic resonance imaging for bone metastases: a systematic review and meta-analysis. J Magn Reson Imaging 34(1):128–135
41. Kwee TC, Takahara T, Niwa T (2010) Diffusion-weighted whole-body imaging with background body signal suppression facilitates detection and evaluation of an anterior rib contusion. Clin Imaging 34:298–301
42. Messiou C, Collins DJ, Morgan VA, Desouza NM (2011) Optimising diffusion weighted MRI for imaging metastatic and myeloma bone disease and assessing reproducibility. Eur Radiol 21:1713–1718
43. Eiber M, Holzapfel K, Ganter C et al (2011) Whole-body MRI including diffusion-weighted imaging (DWI) for patients with recurring prostate cancer: technical feasibility and assessment of lesion conspicuity in DWI. J Magn Reson Imaging 33:1160–1170
44. Bin L, Qiong L, Wei N, Shiyuan L (2014) Diagnostic value of whole-body diffusion-weighted magnetic resonance imaging for detection of primary and metastatic malignancies: a meta-analysis. Eur J Radiol 83(2):338–344
45. Hardie AD, Naik M, Hecht EM, Chandarana H, Mannelli L, Babb JS, Taouli B (2010) Diagnosis of liver metastases: value of diffusion-weighted MRI compared with gadolinium-enhanced MRI. Eur Radiol 20(6):1431–1441
46. Kwast AB et al (2012) Histological type is not an independent prognostic factor for the risk pattern of breast cancer recurrences. Breast Cancer Res Treat 135(1):271–280
47. Montagna E, Peccatori F, Petralia G, Tomasi Cont N, Iorfida M, Colleoni M (2014) Whole-body magnetic resonance imaging, metastatic breast cancer and pregnancy: a case report. Breast 23(3):295–296
48. Oto A, Ernst R, Jesse MK, Chaljub G, Saade G (2007) Magnetic resonance imaging of the chest, abdomen, and pelvis in the evaluation of pregnant patients with neoplasms. Am J Perinatol 24(4):243–250
49. Brenner DJ, Hall EJ (2007) Computed tomography—an increasing source of radiation exposure. N Engl J Med 357(22):2277–2284
50. Kanda T, Ishii K, Kawaguchi H, Kitajima K, Takenaka D (2014) High signal intensity in the dentate nucleus and globus pallidus on unenhanced T1-weighted MR images: relationship with increasing cumulative dose of a gadolinium-based contrast material. Radiology 270(3):834–841
51. Padhani AR, Makris A, Gall P, Collins DJ, Tunariu N, de Bono JS (2014) Therapy monitoring of skeletal metastases with whole-body diffusion MRI. J Magn Reson Imaging 39:1049–1078
52. Messiou C, Collins DJ, Giles S, et al (2011) Assessing response in bone metastases in prostate cancer with diffusion MRI. In Proceedings of 19th annual meeting ISMRM, Montreal, p 336
53. Padhani AR, Koh DM (2011) Diffusion MR imaging for monitoring of treatment response. Magn Reson Imaging Clin N Am 19:181–209
54. Edinger AL, Thompson CB (2004) Death by design: apoptosis, necrosis and autophagy. Curr Opin Cell Biol 16:663–669
55. Messiou C, Collins DJ, Giles S, de Bono JS, Bianchini D, de Souza NM (2011) Assessing response in bone metastases in prostate cancer with diffusion weighted MRI. Eur Radiol 10:2169–2177
56. Hillengass J, Bauerle T, Bartl R et al (2011) Diffusion-weighted imaging for non-invasive and quantitative monitoring of bone marrow infiltration in patients with monoclonal plasma cell disease: a comparative study with histology. Br J Haematol 153: 721–728
57. Chan JH, Peh WC, Tsui EY et al (2002) Acute vertebral body compression fractures: discrimination between benign and malignant causes using apparent diffusion coefficients. Br J Radiol 75:207–214
58. Padhani AR, Van Ree K, Collins DL, D'Sa S, Makris A (2013) Assessing the relationship between bone marrow signal intensity and apparent diffusion coefficient on diffusion weighted MRI. Am J Roentgenol 200(1):163–170
59. Chen WT, Shih TT, Chen RC et al (2002) Blood perfusion of vertebral lesions evaluated with gadolinium-enhanced dynamic MRI: in comparison with compression fracture and metastasis. J Magn Reson Imaging 15:308–314
60. Pui MH, Mitha A, Rae WI, Corr P (2005) Diffusion-weighted magnetic resonance imaging of spinal infection and malignancy. J Neuroimaging 15:164–170